The Effects of Bed Friction on Wave Simulation: Implementation of an Unstructured Third-Generation Wave Model, SWAN

Author(s): S. Mostafa Siadatmousavi, F. Jose, and G. W. Stone

Source: Journal of Coastal Research, 27(1):140-152. 2011.
Published By: Coastal Education and Research Foundation
DOI: 10.2112/JCOASTRES-D-10-00073.1
URL: http://www.bioone.org/doi/full/10.2112/JCOASTRES-D-10-00073.1

Journal of Coastal Research | 27 | 1 | 140–152 | West Palm Beach, Florida | January 2011

The Effects of Bed Friction on Wave Simulation: Implementation of an Unstructured Third-Generation Wave Model, SWAN

S. Mostafa Siadatmousavi, F. Jose, and G.W. Stone

Coastal Studies Institute
Department of Oceanography and Coastal Sciences
Louisiana State University
Baton Rouge, LA 70803, U.S.A.
ssiada1@lsu.edu
felixjose@lsu.edu
gagreg@lsu.edu

ABSTRACT

SIADATMOUSAVI, S.M.; JOSE, F., and STONE, G.W., 2011. The effects of bed friction on wave simulation: implementation of an unstructured third-generation wave model, SWAN. *Journal of Coastal Research,* 27(1), 140–152. West Palm Beach (Florida), ISSN 0749-0208.

Parallel implementation of an unstructured Simulating Waves Nearshore (SWAN) model with the Wave Model (WAM) cycle 4 formulation was used to evaluate the performance of a third-generation wave model over large spatial scales. Data from a network of National Data Buoy Center (NDBC) buoys and the Wave Current Information System (WAVCIS) stations were used to assess the skill of the input and output of the wave model. The simulation results reveal that the underestimation of energy in the low-frequency band (0.12–0.17 Hz) can be ameliorated if the model is calibrated using site specific *in situ* measurements instead of the Pierson-Moskowitz spectra. This process led to more than a 25% decrease in the root mean square error between simulated significant wave height and *in situ* observations. Use of the verified model for the Gulf of Mexico, with bed friction computed from grain-size distribution, as opposed to a default constant bed-friction formulation, showed that the wave height difference can exceed 1.5 m or 40% of local wave height for a large spatial extent during extreme events, such as Hurricane Dennis. In addition, with the use of eddy viscosity bed-friction formulation with usSEABED (U.S. Geological Survey), the sediment data results were in better agreement with the *in situ* observations during Hurricane Dennis, with less than a 4% increase in computational cost. The mean wave-height distribution over several cold fronts also demonstrates the influence of bed grain-size parameterization in wave transformation, especially in water depths shallower than 15 m, thereby demonstrating the significance of this study in advancing our understanding of sediment-transport modeling.

ADDITIONAL INDEX WORDS: *JONSWAP, Madsen bed friction formula, numerical modeling, Hurricane Dennis, Gulf of Mexico, SWAN.*

INTRODUCTION

Third-generation wave models are employed as viable tools to simulate the wave field for medium (order of 50 km) and large-scale (oceanic) domains (Zubier, Panchang, and Demirbilek, 2003). These phase-averaged models include deep water source/sink terms, such as wind input, quadruplet wave–wave interaction, and energy dissipation (Komen *et al.*, 1994), among which dissipation in deep water is widely considered to be the least-understood term (Cavaleri *et al.*, 2007). In third-generation models, the most commonly used formulation for deep water dissipation and wind input, are Wave Model (WAM) cycle 3 (WAM-3) and WAM cycle 4 (WAM-4) (Komen *et al.*, 1994). The WAM-3 employs an empirical formulation for wind input (Komen, Hasselmann, and Hasselmann, 1984; Snyder *et al.*, 1981) and a pulse-based, quasilinear model (Hasselmann, 1974). It has been shown that WAM-3 formulations and nonlinear wave interaction formulation referred to as the Discrete Interaction Approximation (DIA) (Hasselmann *et al.*, 1985) can reproduce a fully developed wind–sea (Komen, Hasselmann, and Hasselmann, 1984). A detailed spectral analysis of WAM-3 and its consistent underprediction of wave-energy levels at lower frequencies are well described in Rogers, Hwang, and Wang (2003). The WAM-4 is the newer equation, based on quasilaminar wind–wave energy transfer with more flexibility in the formulation for whitecapping dissipation (Janssen, 2004). In addition, some models, such as MIKE21-SW, exclusively include WAM-4 formulations (Sørensen *et al.*, 2004). Therefore, a detailed study on the spectral performance of WAM-4 is necessitated to help establish whether this formulation also suffers from the underprediction of the energy density in low frequencies.

When waves propagate across intermediate and shallow waters, wave transformation processes, such as bed friction, become important. In shallow water, bed friction is as important as nonlinear wave–wave interaction (Graber and

DOI: 10.2112/JCOASTRES-D-10-00073.1 received 15 May 2010; accepted in revision 17 August 2010.
Published Pre-print online 12 November 2010.

Madsen, 1988). Bed friction dissipates the energy transfer toward lower frequencies because of nonlinear wave interactions, which leads to the shift in the spectral peak toward higher frequencies (Graber and Madsen, 1988). Although several different formulations have been proposed to include the bed-friction effect in wave models, the simplest approach, referred to as the JONSWAP model (Hasselmann *et al.*, 1973), is generally used because of its simplicity. This formula has been reported successful under many practical conditions (Tolman, 1994). In addition, many wave models' dependence on bottom-sediment size distribution is weak for small domains, such as those of a few kilometers in length and width (Kagan, Alvarez, and Gorchakov, 2008). Moreover, the JONSWAP formula is not a function of bed lithology or fabric characteristics, which makes it more practical to use for large-scale simulations, where a uniform distribution of sedimentological data may not be available for the entire domain. However, the reasonably good sediment-classification study completed by the U.S. Geological Survey (USGS) for the northern Gulf of Mexico (usSEABED) affords a unique opportunity to take advantage of these field measurements to run well-calibrated wave models with more complex bed-friction formulations and the opportunity to evaluate the importance of bed formulation in their performances.

Among different bed-friction models, the Madsen drag-law formulation has been proven to be one of the most accurate bed-friction dissipation models that depend on near-bottom orbital velocity as well as bed roughness (Madsen, Poon, and Graber, 1988). Although considered to be computationally expensive, compared with the JONSWAP method, unlike most eddy-viscosity equations, it scales with friction velocity (Luo and Monbaliu, 1994). This makes it more appropriate for use in the wave-action balance equation of third-generation wave models, such as SWAN (Komen, Hasselmann, and Hasselmann, 1984; Janssen, 2004; Rogers, Hwang, and Wang, 2003).

The purpose of this study was to determine the effects of bed grain-size distribution on simulated wave height. Therefore, as a first objective, the unstructured SWAN model was implemented to further investigate the spectral performance of whitecapping dissipation formulation of the WAM-4 and to determine the most appropriate coefficients to calibrate a regional model for the Gulf of Mexico. The calibrated SWAN model has been used to study the effects of bed-friction formulation and its dependency on bed-sediment distribution in the Gulf of Mexico. Depending on the goal of the wave simulations, quantification of the difference between two bed-friction formulae can be studied by either incrementally changing the mean wave height over a relatively long time (Georgiou and Schindler, 2009; Nielsen, 1992) or changing the wave height during an extreme high-energy event. The former criterion is useful for long-term response studies, such as sediment transport, whereas the latter is more important in studies of hurricane impacts on offshore structures and along the coastline. An additional objective of this study was to perform simulations over a time period of a few discrete cold-front passages during Spring 2007 as well as for an active cold-front season, from December 2007 to April 2008, for the first approach, and during Hurricane Dennis (2005) prelandfall met-ocean conditions for analyzing the second approach.

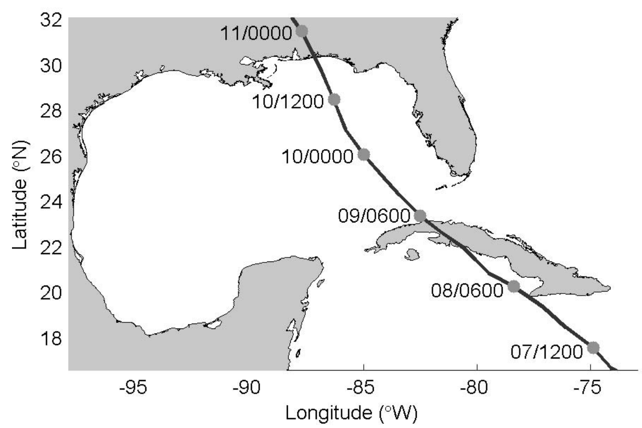

Figure 1. The track of Hurricane Dennis in the Gulf of Mexico (Data courtesy of Beven, 2006).

Hurricane Dennis

Although August and September are generally the most common months for Atlantic hurricanes to form (Grenci and Nese, 2006), Dennis originated from a tropical wave on June 29, 2005, and transformed into a tropical depression on July 4, 2005, near the southern Windward Islands, in the Caribbean. While moving northwestward, it intensified and became a tropical storm on July 5, 2005, and later reached hurricane status on early July 7, 2005. Hurricane Dennis reached Category 4 status before making two successive landfalls in Cuba (see Figure 1) with sustained wind speed of 222 km/h (120 kts) on July 8, 2005. It weakened considerably after crossing Cuba and emerged in the Gulf of Mexico at 0900 hours Coordinated Universal Time (UTC) on July 9, 2005, as a Category 1 hurricane. As it tracked northward, Dennis strengthened, after being significantly influenced by warmer waters from a well-established Loop Current along the eastern Gulf of Mexico, and again became a Category 4 hurricane on July 10, 2005, with wind speeds attaining 231 km/h (125 kts). Because of mid- and upper-level dry air, Dennis weakened to a Category 3 hurricane before final landfall at Navarre Beach, along Santa Rosa Island, Florida, at 1930 hours UTC on July 10, 2005 (Beven, 2005; Morey *et al.*, 2006).

NUMERICAL MODEL: SWAN

Model Physics

The Simulating Waves Nearshore (SWAN) is a third-generation wave model being developed by Delft University of Technology (Booij, Ris, and Holthuijsen, 1999). The model has been used successfully for high-energy events, such as typhoons and tropical storms (Palmsten, 2001; Zhang, Kiu, and Lin, 2003). Similar to other spectral wave models (WAM, WAVEWATCH-III, and MIKE21), SWAN is based on the wave-action conservation equation, which is also valid in the presence of currents (Whitham, 1965). Wave action (N) is defined as $N \equiv E/\sigma$, where E and σ denote wave energy and relative frequency, respectively. Wave propagation is described by the following equation:

$$\frac{DN}{Dt} \equiv \frac{S}{\sigma} \tag{1}$$

where DN/Dt represents the total time derivative of the wave action, and S is composed of all energy sources and sinks. In deep water, S is primarily determined by wind-energy input, quadruplet wave–wave interaction, and whitecapping dissipation; whereas in intermediate and shallow water, depth-induced wave breaking, bed friction, and triad wave–wave interaction effects are also significant. There are several formulations in SWAN that describe each of these sinks and sources. Exponential wave growth and wave dissipation can be taken into account by WAM-4 or WAM-3 formulation (SWAN Team, 2008; WAMDI Group, 1988). Although SWAN's default option is WAM-3 and it is used in several studies (Moeini and Etemad-Shahidi, 2007; Rogers, Hwang, and Wang, 2003;, Rogers *et al.*, 2007; Zijlema and Van der Westhuysen, 2005), we have used WAM-4, in which wave growth is based on quasilaminar wind–wave energy transfer, and wave dissipation allows nonlinear dependency of whitecapping energy loss on the wave number (Komen *et al.*, 1994). The DIA method is employed for quadruplet wave–wave interaction, and depth-induced wave breaking is taken into account by a spectral form of the bore model (Battjes and Janssen, 1978; Eldeberky and Battjes, 1995). Wave dissipation caused by bottom friction is important in shallow water, especially during high-energy events (Li and Mao, 1992) and is roughly estimated as a few watts *per* square meter, approximately the same rate of energy transferred to the sea surface during moderate winds (Cavaleri *et al.*, 2007). In this study, we have implemented both the empirical formulation of JONSWAP (Hasselmann *et al.*, 1973) and the drag-law friction model of Madsen, Poon, and Graber (1988).

Numerical Scheme

Because it was originally developed for wave simulation in shallow water, SWAN employs implicit numerical schemes to avoid extremely small time steps and stability problems. SWAN has three finite-difference schemes for testing, stationary, and nonstationary simulations. In the latest version, SWAN 40.81, a finite-volume scheme is employed, which allows the use of an unstructured, triangular mesh. The computational grid consists of different mesh resolutions, which help the user to optimize the run-time in large-scale models with complex bathymetry. Providing a finer mesh size for the areas of interest and for locations where a sharp change in the wave spectrum is expected, such as shallow water, results in higher accuracy without a tremendous increase in total computational cost.

Mesh File and Mesh Decomposition for Parallel Computation

The BatTri package (Bilgili, Smith, and Lynch, 2006) was used to generate a high-quality mesh file for SWAN. A computational mesh with enough resolution to accommodate the complex bathymetry of shallow water is a prerequisite for coastal wave modeling (Hagen, Horstman, and Bennett, 2002).

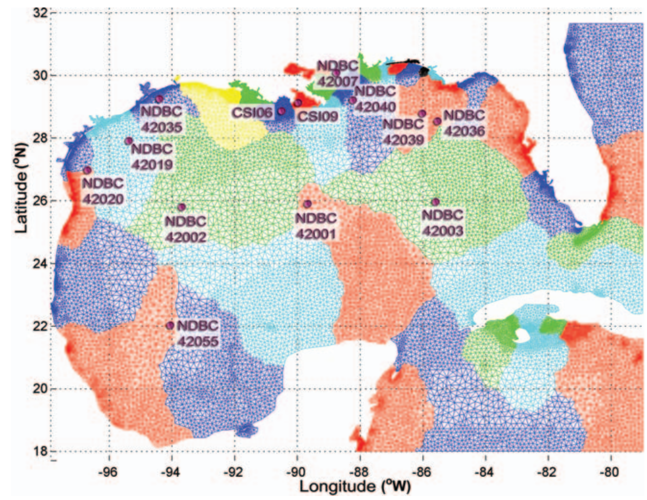

Figure 2. Mesh file and its different partitions for parallel computing using 40 processors. The domain for each CPU has a different color from its adjacent domains. Note that all parts are interconnected subdomains, except the yellow and the black ones, for which one designated processor accomplishes the computations on the disconnected domain. *In situ* observation stations in deep water (NDBC Buoys) and shallow water (WAVCIS CSI stations) used in this study are also included.

In addition, high resolution is assigned to locations where *in situ* data were collected for model-skill assessment. Moreover, to avoid numerical errors, additional precautions were taken, *viz* avoiding steep element slope, very small vertex angles, or even significant change in mesh size relative to the mesh elements nearby (SWAN Team, 2008). The final mesh file used for the study is shown in Figure 2, which consists of 32,235 nodes and 59,258 triangles with the element sides varying from 1 km to 50 km. To run a parallel unstructured SWAN (PunSWAN), the mesh file was partitioned into subgrids and assigned to individual processors. While partitioning the mesh into smaller entities, care was taken to allocate approximately the same number of vertices for each subgrid and the least possible cutting length. This was accomplished using ADCPREP, the grid preparation module of the circulation model ADCIRC (Westerink *et al.*, 1992). Figure 2 also provides the mesh decomposition into 40 parts.

The ratio of computational time for one processor to carry out a task to the time needed for several processors to complete the same task is referred to as *speedup*. SWAN parallel implementation necessitates interdomain communication only for overlapping vertices along the mesh edges (Zijlema, 2009). The PunSWAN shows linear speedup (not shown) on the WAVCISCluster (Wave Current Surge Information System Cluster) (Coastal Studies Institute, 2010) having 20 nodes, each of them having two Intel Xeon CPU 3.06 GHz processors and 2 GB RAM. Linear speedup reaffirms the optimized parallelization of the SWAN source code, which was also reported by Zijlema (2009).

In Situ Observations

Wave, wind, and meteorological archived data from several deep-water buoys obtained from the National Data Buoy

Table 1. *Anemometer elevation (from m.s.l.) at various in situ observation stations.*

	NDBC											WAVCIS	
Station	42001	42002	42003	42007	42019	42020	42035	42036	42039	42040	42055	CSI06	CSI09
Anemometer height (m)	10	10	10	5	5	5	5	5	5	5	10	40	32

Center (NDBC) were analyzed to ascertain the accuracy of the wind field (the main driving force for waves) and the computed deep-water bulk wave parameters from SWAN. Additional data were obtained from WAVCIS stations (Stone *et al.*, 2001), owned and maintained by the Coastal Studies Institute at Louisiana State University, to similarly evaluate the model for shallow waters, where more complex processes, such as bed friction and depth-induced wave breaking, are also important. The locations of *in situ* observations used in this study are given in Figure 2. Table 1 shows that, at some of these stations, sustained wind speed is measured at elevations other than 10 m above the mean sea level (m.s.l.), the unified standard set by the World Meteorological Organization (WMO, 2008). Because SWAN also requires the wind speed at 10 m above m.s.l. (referred to as U_{10}) as input, we converted measured wind speed at elevation z above m.s.l. (referred to as U_z) to U_{10}. The widely accepted conversion formula is based on a logarithmic wind profile (Peixoto and Oort, 1992; Thomas, Kent, and Swail, 2005). The power-law wind profile is another simple method for reconstruction of the wind profile over an offshore water body in a neutral-condition, which is the case for a moderate or strong wind speed that produces a noticeable wind-induced sea state (Hsu, 1988). However, these theories are not valid in unstable conditions nor for very stable conditions (Walmsley, 1988). There are also more complex formulae, such as the LKB model (Liu and Tang, 1996), that take into account the stability state and the effects of temperature and humidity on the wind profile.

Wind Data

Both u and v wind velocity components were extracted from the North American Regional Reanalysis (NARR) database from the National Centers for Environmental Prediction (NCEP) server. The NARR data grid 221 covers the entire continental United States and the Gulf of Mexico with a horizontal resolution of ~32 km. Given that the accuracy of wind data plays an important role in the accuracy of wave hindcasting (Janssen, 2008; Kumar *et al.*, 2000), it is important to evaluate the quality of wind input. The wind speed data from NDBC buoys and the WAVCIS stations were rescaled with the methods discussed earlier, to find the best time period during which all scaling methods show a high correlation between measured and simulated wind speeds. The following statistical parameters are useful in evaluating the agreement of two data sets:

$$Bias = \frac{1}{N}\sum_{i=1}^{N}\left(U^i_{10,NARR} - U^i_{10,obs}\right) \tag{2}$$

$$SI = \frac{\sqrt{\frac{1}{N}\sum_{i=1}^{N}\left(U^i_{10,NARR} - U^i_{10,obs}\right)^2}}{\frac{1}{N}\sum_{i=1}^{N}U^i_{10,obs}} \tag{3}$$

in which N is the number of data points, i is the time index, and $U^i_{10,NARR}$ and $U^i_{10,obs}$ are wind speeds at 10 m above m.s.l. from the NARR database and from the *in situ* observation, respectively. To ensure the model works well in wind–sea generation, the target time period was also required to extend at least 10 days with only few time periods in which wind speed was less than 5 m/s. During the extended time period from December 2006 to April 2007, the last two weeks of March 2007 were finally selected and were referred to as the first time period thereafter. Wind data for another time period, between December 20, 2006, 0000 hours, and January 1, 2007, 0000 hours, were also used to evaluated the sensitivity of model calibration on the quality of wind data. This period was referred to as the second time period thereafter.

In Table 2, the scattering index and bias between NARR wind data and *in situ* observations, averaged over all NDBC stations and WAVCIS stations for the first and second time periods are shown. It is clear that the first time period has lower scatter and bias than the second one. An example of the wind-speed time series at NDBC 42003 and the error in wind data at that station during the first time period is presented in Figure 3. The data show all methods lead to similar results; we used the LKB method because of the inclusion of more physical parameters in that method in the reconstruction of the wind profile.

To prepare wind data for simulating Hurricane Dennis, higher resolution wind data, especially near the center of the hurricane, was necessary. Combining National Oceanic and

Table 2. *Scattering index and bias of wind speed obtained from NARR database and* in situ *observations for the first and second time period using power law (POW), logarithmic wind profile (Log), and LKB model (LKB) to scale measured wind to* U_{10}.

	Statistical parameter					
	Pow		Log		LKB	
Time period	SI	Bias (m/s)	SI	Bias (m/s)	SI	Bias (m/s)
First time interval	0.260	−0.181	0.262	−0.226	0.253	−0.348
Second time interval	0.316	−1.087	0.318	−1.156	0.323	−1.276

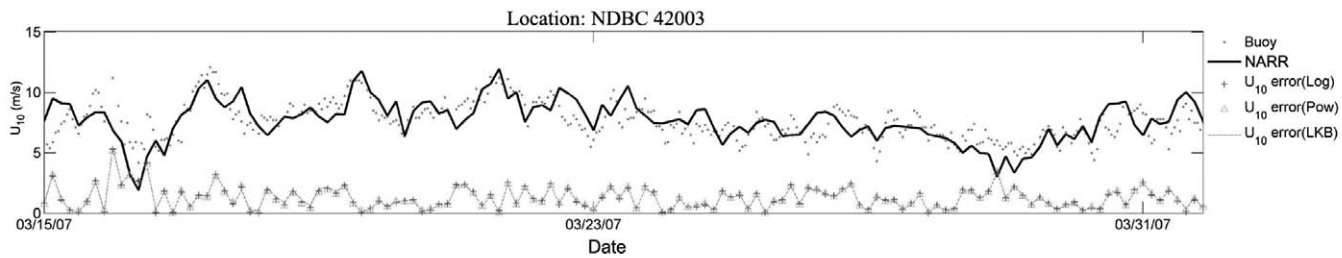

Figure 3. Comparison between NARR-derived wind speed (black line) and *in situ* observation at NDBC 42003 (red dots). Wind speed error using log profile (blue cross), power profile (green triangle), and LKB method (dotted line) for the first time period are also included.

Atmospheric Administration (NOAA)–Hurricane Research Division (HRD) high-resolution reanalyzed wind data (NOAA, 2010) with NARR data provide higher resolution to investigate the dynamics associated with wind asymmetry near the center of hurricanes. The HRD wind data are derived from a synthesis of all available surface-weather platforms, aviation reports, and reconnaissance aircraft data adjusted to the surface, providing 6-km resolution data within the 1,000-km × 1,000-km "moving box" centered around the hurricane's track. Linear interpolation was used in both time and space domains to blend two sets of wind data to prepare wind inputs for SWAN for every 3 hours.

Bathymetry

Bathymetry was downloaded from the National Geophysical Data Center (NGDC). Three-seconds cell size (~90 m) data from the U.S. Coastal Relief Model Grids database for the northern Gulf of Mexico were combined with coarser ETOPO1 1-minute Global Relief database that covered the entire Gulf. MATLAB linear interpolation was used to determine the depth for each mesh node from the best database, and the result was carefully checked to remove any potential anomalies in both databases.

Bed Roughness

The general spectral form of the bed friction term can be expressed as follows:

$$S_{fric}(\sigma,\theta) = -C\frac{\sigma^2}{g^2\sinh^2 kh}E(\sigma,\theta) \tag{4}$$

in which $E(\sigma, \theta)$ is the two-dimensional frequency spectrum, σ is angular frequency, θ is the direction of the wave component, k is the wave number, and h is the local water depth. Coefficient C depends on the friction model used for the computation, and in the simplest model, JONSWAP method, can be considered as the constant value: $C_{JONSWAP} = 0.038$ (Hasselmann *et al.*, 1973). Our sensitivity analysis shows that a 100% increase of $C_{JONSWAP}$ can result in a 5% to 10% decrease in simulated significant wave height (SWH) in coastal stations shown in Figure 2; *i.e.*, WAVCIS stations CSI06 and CSI09 as well as NDBC buoys, which are relatively closer to the coastline, such as 42007, 42019, 42020, and 42035. It has been shown that the coefficient C in Equation (4) is not constant and depends on wave-induced bed velocity (Young and Gorman, 1995). For example, it can be evaluated from more complex models, such as the eddy–viscosity model of Madsen, Poon, and Graber (1988), in which the following set of equations are solved:

$$C_{MADSEN} = \frac{g}{\sqrt{2}}f_w U_{rms} \tag{5}$$

$$U_{rms} = \sqrt{\iint \frac{\sigma^2}{g^2\sinh^2 kh}E(\sigma,\theta)\,d\sigma\,d\theta} \tag{6}$$

where U_{rms} is the root mean square bottom-orbital velocity. Because the flow is usually assumed to be turbulent (Tolman, 1992), the friction factor f_w can be solved by iteration from the following set of equations (Jonsson, 1967):

$$\frac{1}{4\sqrt{f_w}} + \log_{10}\frac{1}{4\sqrt{f_w}} = m_f + \log_{10}\frac{a_b}{K_N} \tag{7}$$

$$a_b = 2\sqrt{\iint \frac{1}{\sinh^2 kh}E(\sigma,\theta)\,d\sigma\,d\theta} \tag{8}$$

in which a_b is the near-bottom excursion amplitude (Madsen, Poon, and Graber, 1988), $m_f = -0.08$ is constant (Jonsson and Carlsen, 1976), and K_N is the bed roughness height and depends on the sediment properties. The term K_N is of the order of $1 - 10\ d_{50}$ for flat beds, in which d_{50} is the median sediment grain size, and of the order of 100 d_{50} in ripple beds (Nielsen, 1992). Moreover, the K_N values ranging between 2 cm and 5 cm were proven to result in satisfactory performance of wave models (Tolman, 1991). Assuming the average value of K_N = 4 cm for typical sand with a median grain size of 0.2 mm, and a linear relationship between K_N and d_{50} leads to $K_N = 200\ d_{50}$, which is the relationship selected in this study. The constant value of 200 used in this study is also very close to the average of the data shown in Figure 3.6.4 of Nielsen (1992). Moreover, the lowest and highest possible values for K_N were set to 0.1 cm and 10 cm, respectively. Because the default bed friction implemented in SWAN is based on a sandy bottom, the above-mentioned filter will effectively replace nonphysical values of K_N, computed from a wide range of sediment-size data. Sensitivity analysis was performed by applying $K_N = 250\ d_{50}$ for the first time period, which led to less than 5% change in SWH at NDBC 42007 (the remaining stations show less SWH change). Note that SWAN also uses $f_w = 0.3$ for values of a_b/K_N smaller than 1.57, instead of the value from Equation (7) (Jonsson, 1980).

usSEABED Database

The usSEABED is a joint effort between the USGS and the University of Colorado, resulting in a compilation of seafloor sediment characteristics around the United States from the beach to the deep waters. The data source includes surficial and subbottom data from physical sampling equipments (grabs and cores) and virtual sampling, such as descriptions based on interpretations of seafloor photographs. The database has already proven to be very effective in Louisiana coastal ecosystem-restoration programs as well as in sediment-mobility studies (Buczkowski *et al.*, 2006). For the study, the sediment grain-size distribution data for the Gulf of Mexico were collected from the usSEABED database. The data on mean grain-size distribution was scarce for the southern half of the Gulf of Mexico. Therefore, the average value of the roughness height for the region north of 24° latitude was calculated and applied for the entire domain south of 24° latitude. This approximation is assumed to have negligible effects on the overall outcome from this study, given that, as will be discussed in later sections, the bed material affects the simulated wave height mainly in shallow water. Hence, the simulated wave parameters from shallow waters south of 24° latitude are rarely included in this study to evaluate the performance of the model. More than 16,000 data points, predominantly concentrated along the shallow U.S. coastal water, are used for interpolation of d_{50}, ranging from very fine clay to coarse sand; however, most of the samples were within the range of very fine silt to medium sand.

Whitecapping

The physics of whitecapping is not fully understood, and there are several theories and formulations available to include it in third-generation wave models (Babanin *et al.*, 2010; Cavaleri *et al.*, 2007; Rogers, Hwang, and Wang, 2003; Tolman and Chalikov, 1996; Van der Westhuysen, Zijlema, and Battjes, 2007). As discussed earlier, the WAM-4 formulation of SWAN has been used in this study in which energy dissipation due to whitecapping can be expressed as follows:

$$S_{wc}(\sigma,\theta) = -C_{ds}\left[(1-\delta)+\delta\frac{k}{k_m}\right]\left(\frac{s}{s_{PM}}\right)^m \sigma_m\frac{k}{k_m}E(\sigma,\theta) \quad (9)$$

in which s is the wave steepness, subscript PM denotes a fully developed condition (Pierson and Moskowitz, 1964), and σ_m and k_m denote mean angular frequency and mean wave number. The steepness parameter $m = 2$ is used according to Komen *et al.* (1994) to ensure reproduction of deep-water fully developed spectrum. Therefore, the only remaining parameters to tune the model are C_{ds} and δ, and their default values are 4.5 and 0.5, respectively.

Model Calibration

The main calibration parameters for wave models in deep water are tuning parameters C_{ds} and δ for whitecapping energy dissipation. These parameters are originally set to have the best possible agreement with the Pierson-Moskowitz (PM) spectrum (Pierson and Moskowitz, 1964). However, this approach was criticized by Rogers, Hwang, and Wang (2003), who argued that model results achieve energy levels of the PM spectrum very slowly. Moreover, that study affirmed that the model formulations scale according to wind-shear velocity, whereas the PM spectrum scales in accord with U_{10}. In this study, following Rogers, Hwang, and Wang (2003), the best values for dissipation tuning parameters were determined by minimizing the root mean square error (RMSE) of SWH by changing C_{ds} from 1 to 4.5 (0.5 increments) and δ from 0.1 to 0.9 (0.2 increments).

Model Verification

Two simulations with SWAN, using new values for whitecapping parameters and using the default values, were carried out for the period of December 2007 to April 2008, which contained several cold front events as well as intermittent fair weather (calm) periods. Simulation of waves for such extended periods of time (~5 mo) could ensure better performance of SWAN using parameters already determined from the calibration process.

RESULTS AND DISCUSSION

The RMSE for all stations, calculated and averaged for each combination of C_{ds} and δ for the first time interval, are shown in Figure 4A. It is evident that the default values of C_{ds} and δ cannot reproduce the best match between measurement and simulation (see the black dot). The sensitivity of wave height to δ is not as strong as its sensitivity to C_{ds}. The minimum error was found when the tuning parameters were set to $C_{ds} = 2.0$ and $\delta = 0.7$ (the white dot). To investigate the sensitivity of the analysis on the accuracy of wind data, a similar calculation has been completed for the second time period. Figure 4B illustrates that, although wind data accuracy is not as good as in the first time period, $C_{ds} = 2.0$ and $\delta = 0.7$ is very close to the optimum values. The averaged RMSE is reduced by 25% and 35%, after using the optimum values for tuning parameters for the first and second time periods, respectively, instead of using the default values. Qualitative comparison between SWAN hindcast and *in situ* data, such as shown in Figure 5, demonstrates that the model is successful in reproducing the general wave characteristics and that the model calibration using *in situ* observations could significantly ameliorate an underestimation of SWH resulting from a PM calibration of SWAN.

The scatter plot of simulated SWH *vs. in situ* observations from all stations shown in Figure 2, for the period of December 2007 to April 2008, is used for verification of the calibrated model. The linear regression (gray line) in the left panel of Figure 6 shows that the PM-calibrated model significantly underestimates SWH. The bias of the data shown in Panel A is −0.28 m, and the scattering index (SI) is 0.36. The underestimation of SWH is ameliorated by the new values determined from *in situ* calibration (see the right panel). The statistics confirm the significant improvement of the simulated result in Panel B, in which bias is −0.07 m and SI is 0.29.

The SI of the SWH is plotted against the SI of the wind speed (using the LKB method) in Figure 7, for the first time period at all operating stations. As a general trend, the larger the SI in

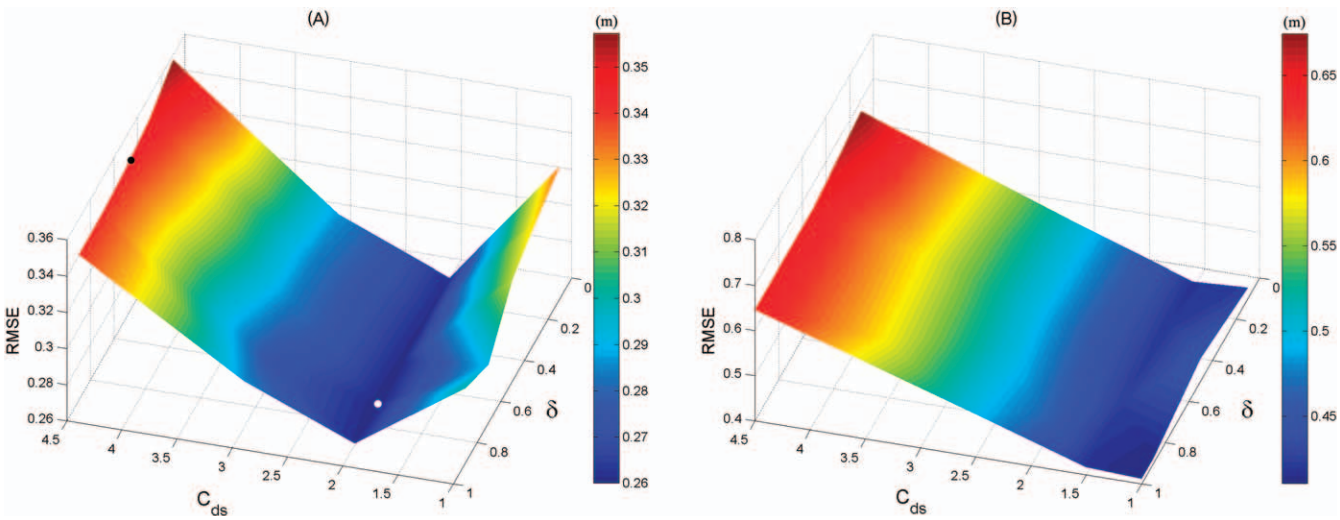

Figure 4. The averaged RMSE for simulated wave height based on whitecapping tuning coefficients, C_{ds} and δ, for (A) the first time period, and (B) second time period. The white dot in panel (A) shows the point of minimum RMSE, and the black dot represents the averaged RMSE corresponding to model calibration using the PM spectrum.

the wind, the larger the SI in wave predictions, which suggests the importance of high-quality wind data in wave hindcasting. However, it is also important to note that the wave SI is less than the wind SI. This could explain why the optimal parameters in Figure 4 are not critically sensitive to the quality of wind data.

Figure 8 demonstrates that using the default values of the tuning parameters for whitecapping dissipation leads to a persistent underestimation of the energy in the frequency band between 0.12 Hz and 0.17 Hz. However, this frequency band is narrower than the frequency band of 0.05–0.19 Hz, in which the WAM-3 formulation shows consistent underestimation (Rogers, Hwang, and Wang, 2003). The lower panel shows that the calibration process amends the severity of the general underestimation in this frequency band but also leads to a slight overestimation of the energy level at frequencies between 0.1 Hz and 0.12 Hz. This overestimation may be the result of using the DIA for nonlinear interaction. Although it is computationally efficient, the DIA method yields a fairly inaccurate representation of energy transfer between wave components (Van Vledder and Bottema, 2003). The DIA transfers more energy to the frequencies lower than the peak frequency (Hasselmann *et al.*, 1985), which results in a broader spectrum (Tolman and Chalikov, 1996).

The mean SWH was calculated during the entire first period, using both JONSWAP and the Madsen, Poon, and Graber (1988) formulae, to determine the effect of the friction formula on bulk-wave parameters. The maximum SWH computed using either of the two methods was approximately 3 m, and the average SWH of hourly outputs over the entire Gulf of Mexico was approximately 1.2 m. The absolute value of the difference between hourly averaged SWH over the entire Gulf of Mexico using two different formulations of bed friction is depicted in Figure 9. It shows that change in the average SWH can exceed 15% of the averaged wave height (shown in red) at isolated locations, *viz*, Golfo de Batabano, Cuba; Waccasassa Bay, Florida Gulf Coast; and the south-central Louisiana coast. Although the bed-friction effect is considered important for shallow-water wave transformation when $k_p h < \pi$ (Young and Gorman, 1995) (in which k_p is the peak wave number), it is also

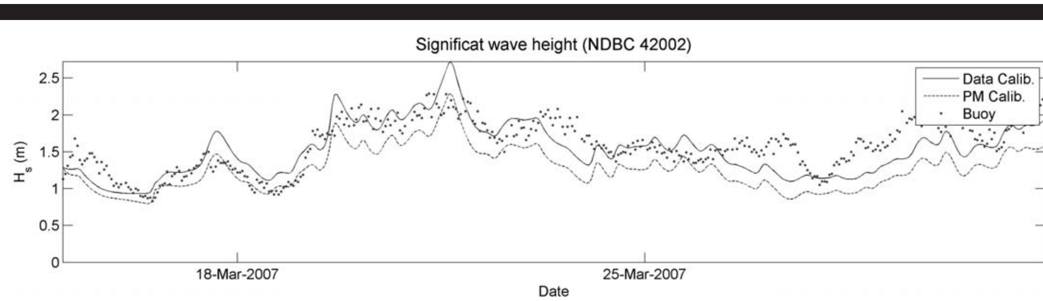

Figure 5. Significant wave height from NDBC 42002 and corresponding hindcast output using SWAN calibrated to the *in situ* data (black solid line) and to the PM spectrum (blue dash line) during the first time period.

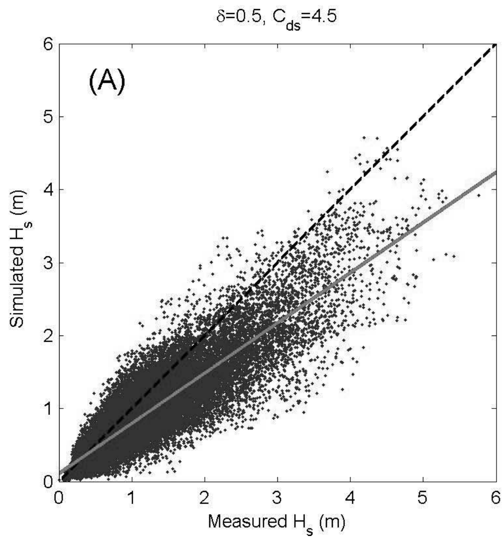

Figure 6. Scatter plot of simulated wave height *vs. in situ* measurements for all stations shown in Figure 1, during 5 mo of simulation using SWAN calibrated to (A) the PM spectrum, and (B) the *in situ* data. The gray lines represent linear regression through data, and the black dash line is the reference line.

important regarding the interrelationship between the characteristics of bed materials and the water depth. This approach implicitly includes hydrodynamic conditions because it depends on the simulated wave fields during the study period. However, it is more convenient to present it by the influence of water depth in which one should also expect the complex interaction of waves with bed-sediment characteristics. Comparing 15-m isobaths with contours of 5% and 10% change in the mean SWH, shows that the region of significant change in mean SWH is mainly shallower than 15 m. However, along the Waccasassa Bay, west of Florida, the 5% change extends to the 20-m isobath.

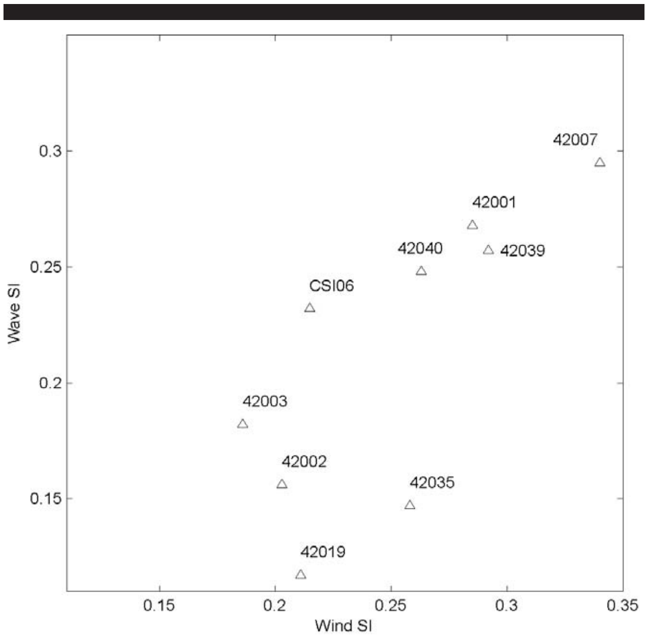

Figure 7. The scattering index of the wave *vs.* scattering index of the wind for all stations in which data were available during first time period.

To have a better understanding of the importance of the bottom-friction formulation in the wave models, the SWH distribution was simulated when Hurricane Dennis moved across the Gulf of Mexico. Figure 10A presents the wave-height distribution at 0000 hours UTC on July 10, 2005, when Hurricane Dennis was located off the southwest coast of Florida (see Figure 1 for the hurricane trajectory). The difference between computed wave height using JONSWAP and Madsen's bed-friction formulations is provided in Figure 10B. It is evident that the JONSWAP formulation generally resulted in higher wave heights than the Madsen formulation. Moreover, the difference between the two formulations is spatially extensive, and a wave-height difference of 1.5 m is observed near the Waccasassa Bay, west Florida. Panel C shows that the relative change in wave height can exceed 25% along the coast in water depths less than 30 m. During extreme weather events, such as Hurricane Dennis, the relative difference of 40% can be found in water depths shallower than 15 m. Note that 15 hours later, when Hurricane Dennis moved closer to the Florida Panhandle, the difference between both formulations remained substantial.

Although *in situ* wave data were not available along the Florida Gulf Coast during Hurricane Dennis, directional wave data from CSI06, off the south-central Louisiana coast, were analyzed (Panel F) for that duration. The data from CSI06 were further used to evaluate the performance of bed formulations, and the results are presented in Figure 11. The WAVCIS stations are equipped with both ADCP (Acoustic Doppler Current Profiler) and Paroscientific pressure sensors, and the good agreement between two data sets

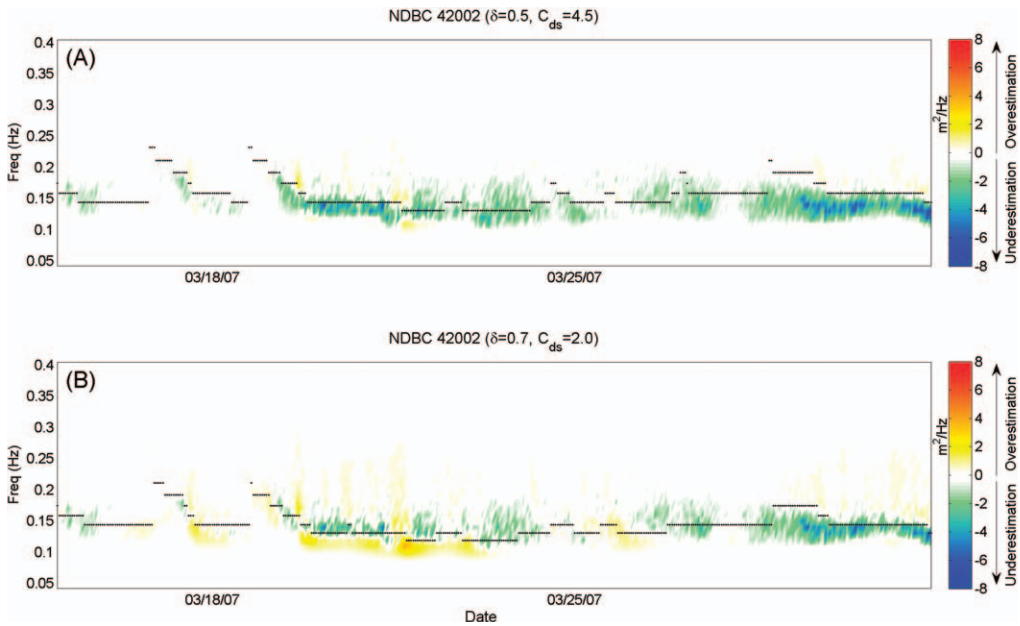

Figure 8. The difference between energy level (as a function of time and frequency) measurements at NDBC 42002 and simulations, using SWAN calibrated to (A) the PM spectrum, and (B) the *in situ* data. The black dots represent simulated peak-wave period.

guarantees the accuracy and reliability of *in situ* observations from this program. Note that both formulations result in the same values for SWH during fair-weather conditions at this station. However, as SWH increases and wave interaction with the bottom increases, the difference between the simulated SWH using the two methods increases. After a few hours, the SWH decreases; hence, the effect of bed friction on wave propagation decreases considerably, and the simu-

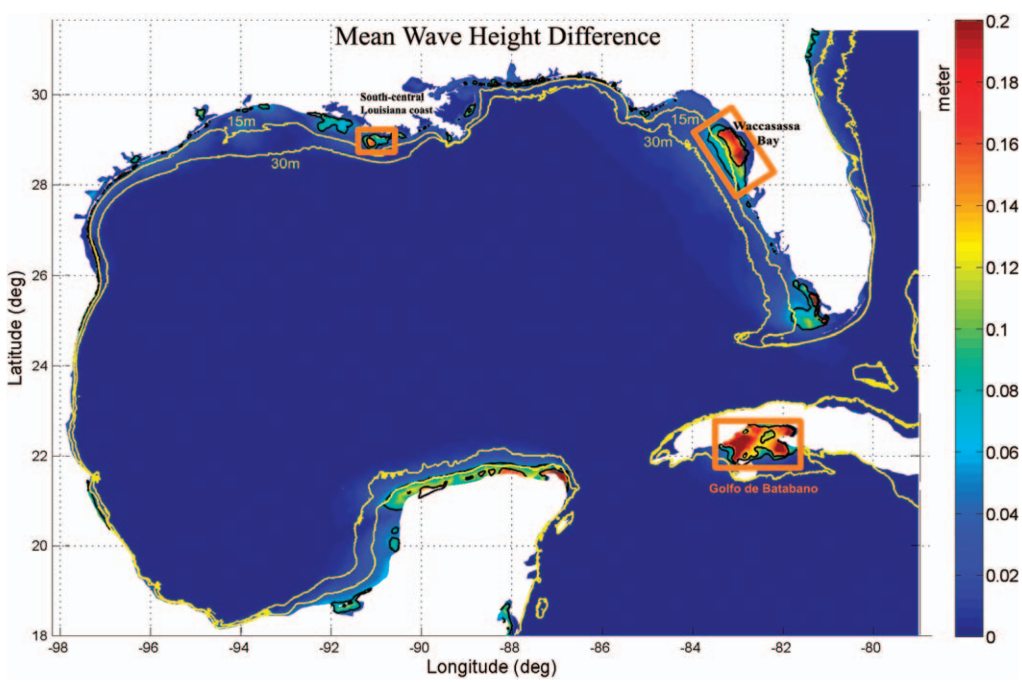

Figure 9. Change in hourly averaged, significant wave height over the entire Gulf of Mexico. Black lines show contours of 5% and 10% change in significant wave height, and yellow contours represent the 15-m and 30-m isobaths. The boxes show the locations where significant changes in simulated, mean, significant wave heights were computed.

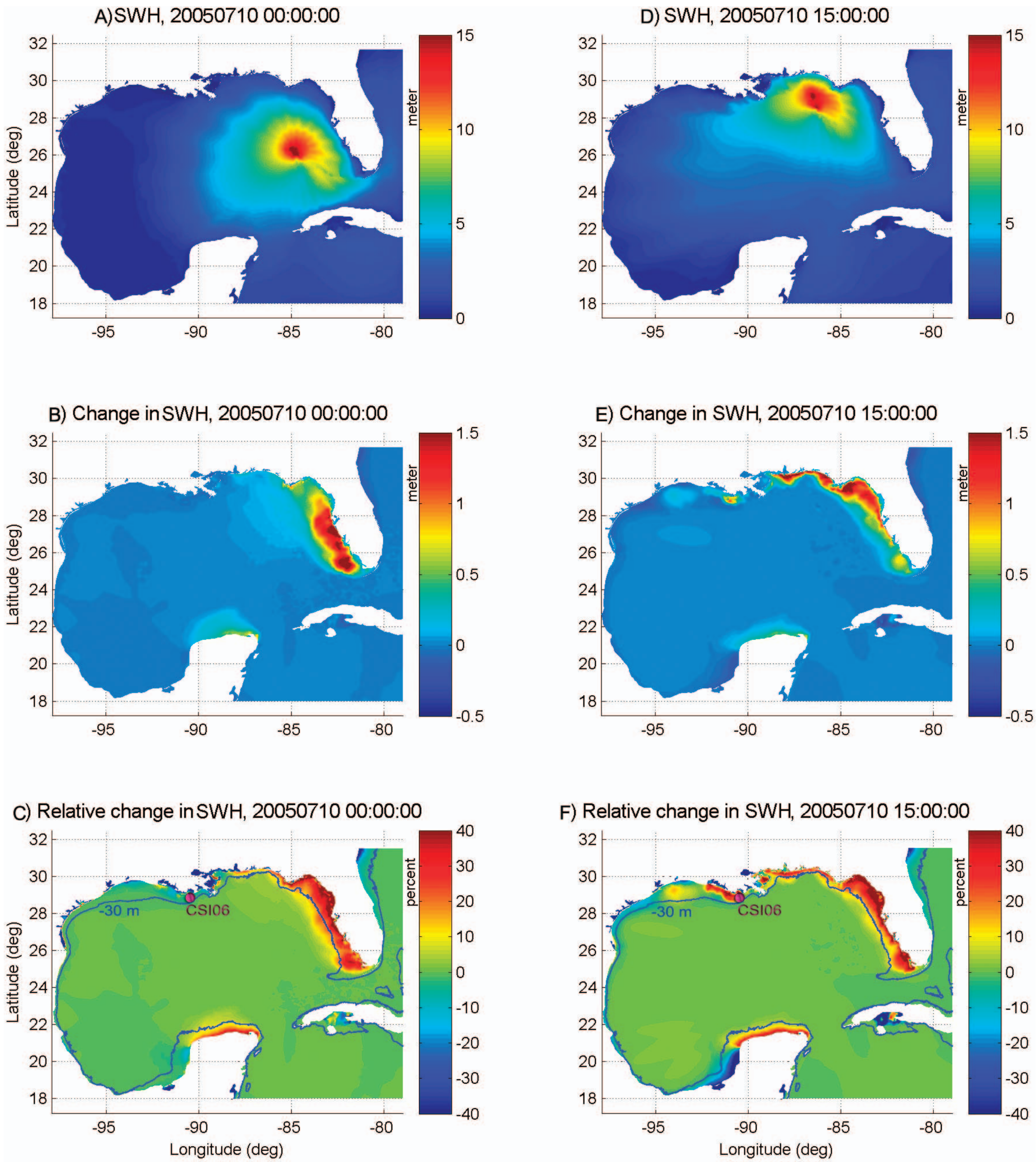

Figure 10. Wave-height simulation results during Hurricane Dennis. Left panels: (A) the significant wave height using the JONSWAP bed formulation, (B) the difference in significant wave height using the Madsen bed-friction formulation instead of the JONSWAP formulation, and (C) the relative wave-height difference between the two bed-friction methods. Right panels are similar to left panels, except with results from 15 h later. Blue lines in C and F are 30-m isobaths.

lated SWH from the two formulations becomes similar again. Based on the research presented here, the bed-friction formulation of Madsen, Poon, and Graber (1988) is in better agreement with *in situ* observations secured during this storm event than that of the JONSWAP formulation. It is also important to note that use of the Madsen model for bed friction in the simulation took an additional 4% of computational time when compared with the JONSWAP formulation.

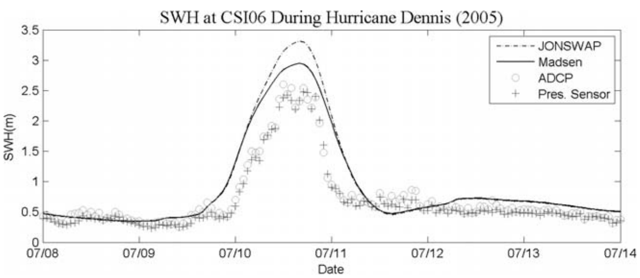

Figure 11. Comparison between hindcast significant wave height at WAVCIS station CSI06 during Hurricane Dennis, computed using the JONSWAP and Madsen bed-friction formulations in SWAN. Measured data from ADCP and pressure sensor at CSI06 are also provided.

CONCLUSIONS

The latest version of the third-generation wave model SWAN was implemented on an unstructured mesh grid to simulate wave fields generated from cold fronts and during the approaching phase of Hurricane Dennis. Measured wind speed and bulk wave parameters from deep-water NDBC buoys and shallow-water WAVCIS stations were used to evaluate the quality of wind input to the wave models and also for quantifying the performance of the wave models. In this study, we have demonstrated the significance of the use of *in situ* observations for fine-tuning the whitecapping process in WAM-4 formulation. For calibrating the tuning parameters for whitecapping, employing observation data can reduce the RMSE in simulated SWH by more than 25%. The accuracy of wave hindcasts is also shown to be critically dependent on the quality of the wind data; however, the best whitecaping coefficients were not sensitive to wind quality. The relatively low scattering index and bias coefficients in both shallow-water and deep-water measurements, showed the capability of the calibrated SWAN model to simulate the wave field over the entire Gulf of Mexico.

Spectral evolution of energy showed that, similar to the WAM-3 formulation, the WAM-4 formulation also suffers from underestimation of energy in the low-frequency band (0.12–0.17 Hz). Calibration of the whitecapping term of the model using *in situ* observations, instead of the PM spectrum, can remedy part of this underestimation. However, doing so also results in a slight overestimation of energy levels in the frequency band between 0.1–0.12 Hz, most likely because of DIA inaccuracy.

The verified model was used to study the effect of bed-friction formulations and the advantage of using the bed-sediment characteristics in wave-height computations. The results show that the JONSWAP bed-friction model with default values generally underestimates the energy dissipation due to bed friction, which results in an overestimation of SWH in shallow water. During severe storms and hurricanes, such as Hurricane Dennis, the difference between JONSWAP and the Madsen, Poon, and Graber (1988) formulations can exceed 1.5 m or 40% of local wave height. The spatial extension of the difference between two formulations depends on the intensity of the wave field and that effect can exceed beyond (seaward) of the 30-m isobath. However, in terms of average wave height during fair-weather and storm conditions, that effect becomes largely confined to shallower water, *i.e.*, landward of the 15-m isobath. These findings have significant implications for further understanding surf-zone processes and innershelf sediment transport. The study also shows that using the Madsen, Poon, and Graber (1988) formulation with usSEABED sediment data results in a superior hindcast with negligible increase in computational time needed to perform the simulations.

ACKNOWLEDGMENTS

We wish to thank Dr. Marcel Zijlema for sharing the source code of the unstructured SWAN. Yixin Luo from the WAVCIS Laboratory, Louisiana State University, set up the WAVCIS Cluster used for the parallel implementation of SWAN for this study. We are also thankful for valuable comments made on an earlier draft from Amy L. Spaziani, Louisiana State University. Jonathan R. Shewchuk (UC-Berkeley) is gratefully acknowledged for providing the triangle-grid generation tool. This study was supported by funding from the Shell Oil Company.

LITERATURE CITED

Babanin, A.V.; Tsagareli, K.N.; Young, I.R., and Walker, D.J., 2010. Numerical investigation of spectral evolution of wind waves, part II: dissipation term and evolution tests. *Journal of Physical Oceanography*, 40, 667–683.

Battjes, J.A. and Janssen, J.P.F.M., 1978. Energy loss and set-up due to breaking of random waves. *In: Proceedings of the 16th International Conference on Coastal Engineering* (Hamburg, Germany, ASCE), pp. 1978. 569–587.

Beven, J.L., 2005. Tropical Cyclone Report: Hurricane Dennis. Miami, Florida: National Hurricane Center.

Bilgili, A.; Smith, K.W., and Lynch, D.R., 2006. BatTri: a two-dimensional bathymetry-based unstructured triangular grid generator for finite element circulation modeling. *Computers & Geosciences*, 32, 632–642.

Booij, N.; Ris, R.C., and Holthuijsen, L.H., 1999. A third-generation wave model for coastal regions, 1: model description and validation. *Journal of Geophysical Research*, 104, 7649–7666.

Buczkowski, B.J.; Reid, J.A.; Jenkins, C.J.; Reid, J.M.; Williams, S.J.. and Flocks, J.G., 2006. usSEABED: Gulf of Mexico and Caribbean (Puerto Rico and U.S. Virgin Islands) offshore surficial sediment data release. Reston, Virginia: U.S. Geological Survey Data Series 146, version 1.0.

Cavaleri, L.; Alves, J.-H.G.M.; Ardhuin, F.; Babanin, A.; Banner, M.; Belibassakis, K.; Benoit, M.; Donelan, M.; Groeneweg, J.; Herbers, T.H.C.; Hwang, P.; Janssen, P.A.E.M.; Janssen, T.; Lavrenov, I.V.; Magne, R.; Monbaliu, J.; Onorato, M.; Polnikov, V.; Resio, D.; Rogers, W.E.; Sheremet, A.; Mckee Smith, J.; Tolman, H.L.; Van Vledder, G.; Wolf, J., and Young, I., 2007. Wave modelling: the state of the art. *Progress in Oceanography*, 75, 603–674.

Coastal Studies Institute, 2010. Wave–current–surge information for coastal Louisiana. Baton Rouge, Louisiana: School of Coast and Environment, Louisiana State University. http://www.wavcis.lsu.edu (accessed June 1, 2010).

Eldeberky, Y. and Battjes, J.A., 1995. Parametrisation of triad interactions in wave energy models. *In:* W.R. Dally and R.B. Zeidle (eds.), *Proceedings of Coastal Dynamics '95: Coastal Research in Terms of Large Scale Experiments*. (Gdansk, Poland, ASCE). pp. 140–148.

Georgiou, I.Y. and Schindler, J.K., 2009. Wave forecasting and longshore sediment transport gradients along a transgressive barrier island: Chandeleur Islands, Louisiana. *Geo-Marine Letters*, 29, 467–476.

Graber, H.C. and Madsen, O.S., 1988. A finite-depth wind-wave model, part 1: model description. *Journal of Physical Oceanography*, 18, 1465–1483.

Grenci, L.M. and Nese, J.M., 2006. *A World of Weather: Fundamental of Meteorology*, Dubuque, Iowa: Kendall/Hunt Publishing Company.

Hagen, S.C.; Horstman, O., and Bennett, R.J., 2002. An unstructured mesh generation algorithm for shallow water modeling. *International Journal of Computational Fluid Dynamics*, 16, 83–91.

Hasselmann, K., 1974. On the spectral dissipation of ocean waves due to whitecapping. *Boundary-Layer Meteorology*, 6, 107–127.

Hasselmann, K.; Barnett, T.P.; Bouws, E.; Carlson, H.; Cartwright, D.E.; Enke, K.; Ewing, J.A.; Gienapp, H.; Hasselmann, D.E.; Kruseman, P.; Meerburg, A.; Müller, P.; Olbers, D.J.; Richter, K.; Sell, W., and Walden, H.. 1973. Measurements of wind-wave growth and swell decay during the Joint North Sea Wave Project (JONSWAP). *Deutsche Hydrographische Zeitschri Supplement A*, 8(12) 95p.

Hasselmann, S.; Hasselmann, K.; Allender, J.H.. and Barnett, T.P., 1985. Computations and parameterizations of the nonlinear energy-transfer in a gravity-wave spectrum, part 2: parameterizations of the nonlinear energy-transfer for application in wave models. *Journal of Physical Oceanography*, 15, 1378–1391.

Hsu, S.A., 1988. *Coastal Meteorology*. San Diego, California: Academic Press, 415p.

Janssen, P.A.E.M., 2004. *The Interaction of Ocean Waves and Wind*. Cambridge, U.K.: Cambridge University Press, 308p.

Janssen, P.a.E.M. 2008. Progress in ocean wave forecasting. *Journal of Computational Physics*, 227, 3572–3594.

Jonsson, I.G., 1967. Wave boundary layers and friction factors. *In: Proceedings of Tenth Conference on Coastal Engineering*. (Tokyo, Japan, ASCE), pp. 127–148.

Jonsson, I.G., 1980. New approach to oscillatory rough turbulent boundary-layers. *Ocean Engineering*, 7, 109–152.

Jonsson, I.G. and Carlsen, N.A., 1976. Experimental and theoretical investigations in an oscillatory turbulent boundary layer. *Journal of Hydraulic Research*, 14, 46–60.

Kagan, B.A., Alvarez, O., and Gorchakov, E.V., 2008. Weak dependence of the SWAN wave model on hydrodynamic properties of sea bottom. *Izvestiya Atmospheric and Oceanic Physics*, 44, 781–786.

Komen, G.J.; Cavaleri, L.; Donelan, M.; Hasselmann, K.; Hasselmann, S., and Janssen, P.A.E.M., 1994. *Dynamics and Modelling of Ocean Waves*, Cambridge, U.K.: Cambridge University Press.

Komen, G. J.; Hasselmann, S., and Hasselmann, K., 1984. On the existence of a fully-developed wind-sea spectrum. *Journal of Physical Oceanography*, 14, 1271–1285.

Kumar, R.; Sarkar, A.; Aggarwal, V.K.; Bhatt, V.; Bhaskaran, P.K., and Dube, S.K., 2000. Ocean wave model: sensitivity experiments. *In: Proceedings of the 5th International Conference PORSEC-2000* Volume 2. (Goa, India, NIO), pp. 621–627.

Li, C.W. and Mao, M., 1992. Spectral modeling of typhoon-generated waves in shallow waters. *Journal of Hydraulic Research*, 30, 611–622.

Liu, W.T. and Tang, W., 1996. Equivalent neutral wind. *JPL Publication*, 96–17, 16p.

Luo, W. and Monbaliu, J., 1994. Effects of the bottom friction formulation on the energy-balance for gravity-waves in shallow-water. *Journal of Geophysical Research-Oceans*, 99, 18501–18511.

Madsen, O.S., Poon, Y.-K., and Graber, H.C., 1988. Spectral wave attenuation by bottom friction: theory. *In:* Edge, B.L. (ed.) *Proceedings of the International Twenty-First Coastal Engineering Conference* (Coata del Sol-Malaga, Spain, ASCE), pp. 492–504.

Moeini, M.H. and Etemad-Shahidi, A., 2007. Application of two numerical models for wave hindcasting in Lake Erie. *Applied Ocean Research*, 29, 137–145.

Morey, S.L.; Baig, S.; Bourassa, M.A.; Dukhovskoy, D.S., and O'Brien, J.J., 2006. Remote forcing contribution to storm-induced sea level rise during Hurricane Dennis. *Geophysical Research Letters*, 33, L19603, 5p. doi:10.1029/2006GL027021.

Nielsen, P., 1992. *Coastal Bottom Boundary Layer and Sediment Transport*. River Edge, New Jersey: World Scientific Publishing Co., 340p.

NOAA (National Oceanic and Atmospheric Administration), 2010. Hurricane Research Division. http://www.aoml.noaa.gov/hrd (accessed February 14, 2010).

Palmsten, M.L., 2001. Application of SWAN Wave Model to a High-Energy Continental Shelf. Tampa, Florida: University of South Florida, Master's thesis.

Peixoto, J.P. and Oort, A.H., 1992. *Physics of Climate*. New York, New York: American Institute of Physics. 520p.

Pierson, W.J. and Moskowitz, L., 1964. A proposed spectral form for fully developed wind seas based on similarity theory of S. A. Kitaigorodskii. *Journal of Geophysical Research*, 69, 5181–5190.

Rogers, W.E.; Hwang, P.A., and Wang, D.W., 2003. Investigation of wave growth and decay in the SWAN model: three regional-scale applications. *Journal of Physical Oceanography*, 33, 366–389.

Rogers, W.E.; Kaihatu, J.M.; Hsu, L.; Jensen, R.E.; Dykes, J.D., and Holland, K.T., 2007. Forecasting and hindcasting waves with the SWAN model in the Southern California Bight. *Coastal Engineering*, 54, 1–15.

Snyder, R.L.; Dobson, F.W.; Elliott, J.A., and Long, R.B., 1981. Array measurements of atmospheric-pressure fluctuations above surface gravity-waves. *Journal of Fluid Mechanics*, 102, 1–59.

Sørensen, O.R.; Kofoed-Hansen, H.; Rugbjerg, M., and Sørensen, L.S., 2004. A third-generation spectral wave model using an unstructured finite volume technique. *In:* Smith, J.M. (ed.) *Proceedings of the 29th International Conference on Coastal Engineering*. (Lisbon, Portugal, ASCE), pp. 894–906.

Stone, G.W.; Zhang, X.P.; Gibson, W., and Frederichs, R., 2001. A new wave-current online information system for oil spill contingency planning (WAVCIS). *In: Proceedings of the 24th Arctic and Marine Oil Spill Program Technical Seminar* (Edmonton, Alberta, Canada, Environment Canada), pp. 401–425.

SWAN Team, 2008. *SWAN Cycle III Version 40.72 Technical Documentation*. Delft, The Netherlands: Delft University of Technology.

Thomas, B.R.; Kent, E.C., and Swail, V.R., 2005. Methods to homogenize wind speeds from ships and buoys. *International Journal of Climatology*, 25, 979–995.

Tolman, H.L., 1991. A third-generation model for wind waves on slowly varying unsteady, and inhomogeneous depths and current. *Journal of Physical Oceanography*, 21, 782–797.

Tolman, H.L., 1992. An evaluation of expressions for wave energy-dissipation due to bottom friction in the presence of currents. *Coastal Engineering*, 16, 165–179.

Tolman, H.L., 1994. Wind-waves and moveable-bed bottom friction. *Journal of Physical Oceanography*, 24, 994–1009.

Tolman, H.L. and Chalikov, D., 1996. Source terms in a third-generation wind wave model. *Journal of Physical Oceanography*, 26, 2497–2518.

Van der Westhuysen, A.J.; Zijlema, M., and Battjes, J.A., 2007. Nonlinear saturation-based whitecapping dissipation in SWAN for deep and shallow water. *Coastal Engineering*, 54, 151–170.

Van Vledder, G. and Bottema, M. 2003. Improved modelling of nonlinear four-wave interactions in shallow water. *In:* Smith, J.M. (ed.), *Proceedings of the 28th International Conference on Coastal Engineering: Solving Coastal Conundrums* (Cardif, Wales, ASCE), pp. 459–471.

Walmsley, J.L., 1988. On Theoretical Wind-Speed and Temperature Profiles over the Sea with Applications to Data from Sable-Island, Nova-Scotia. *Atmosphere-Ocean*, 26, 203–233.

WAMDI Group, 1988. The WAM model—A third generation ocean wave prediction model. *Journal of Physical Oceanography*, 18.

Westerink, J.J.; Luettich, R.A.; Baptista, A.M.; Scheffner, N.W., and Farrar, P., 1992. Tide and storm-surge predictions using finite-element Model. *Journal of Hydraulic Engineering*, 118, 1373–1390.

Whitham, G.B., 1965. A general approach to linear and non-linear dispersive waves using a Lagrangian. *Journal of Fluid Mechanics*, 22, 273–283.

WMO (World Meteorological Organization), 2008. *Guide to Meteorological Instruments and Methods of Observation: Measurement of Surface Wind*. Geneva, Switzerland: Commission for Instruments and Methods of Observation.

Young, I.R. and Gorman, R.M., 1995. Measurements of the evolution of ocean wave spectra due to bottom friction. *Journal of Geophysical Research-Oceans*, 100, 10987–11004.

Zhang, D.L.; Kiu, H., and Lin, P., 2003. The application of SWAN to the simulation of a storm surge. *Proceedings of the International Conference on Estuaries and Coasts* (Hangzhou, China, IAHR).

Zijlema, M., 2009. Multiscale simulations using unstructured mesh SWAN model for wave hindcasting in the Dutch Wadden Sea. *In:* Mizuguchi, M. and Sato, S. (eds.), *Proceedings of Coastal Dynamics: Impacts of Human Activities on Dynamic Coastal Processes* (Tokyo, Japan, ASCE), pp. 1–12.

Zijlema, M. and Van Der Westhuysen, A.J., 2005. On convergence behaviour and numerical accuracy in stationary SWAN simulations of nearshore wind wave spectra. *Coastal Engineering*, 52, 237–256.

Zubier, K.; Panchang, V., and Demirbilek, Z., 2003. Simulation of waves at duck (North Carolina) using two numerical models. *Coastal Engineering Journal*, 45, 439–469.